European Cells and Materials Vol. 40 2020 (pages 189-202) DOI: 10.22203/eCM.v040a12 ISSN 1473-2262

MEASURING MINERALISED TISSUE FORMATION AND RESORPTION IN A HUMAN 3D OSTEOBLAST-OSTEOCLAST CO-CULTURE MODEL

S. Remmers, D. Mayer, J. Melke, K. Ito and S. Hofmann*

Orthopaedic Biomechanics, Department of Biomedical Engineering and Institute for Complex Molecular Systems, Eindhoven University of Technology, Eindhoven, the Netherlands

Abstract

In vitro tissue engineered bone constructs have been developed, but models which mimic both formation and resorption in parallel are still lacking. To be used as a model for the bone remodeling process, the formation and resorption of mineralised tissue volume over time needs to be visualised, localised and quantified. The goal of this study was to develop a human 3D osteoblast-osteoclast co-culture in which 1) osteoblasts deposit mineralised matrix, 2) monocytes differentiate into resorbing osteoclasts, and 3) the formation and resorption of mineralised matrix could be quantified over time using micro-computed tomography (μCT). Mesenchymal stromal cells were seeded on silk fibroin scaffolds and differentiated towards osteoblasts to create mineralised constructs. Thereafter, monocytes were added and differentiated towards osteoclasts. The presence of osteoblasts and osteoclasts was confirmed using immunohistochemistry. Osteoclastic activity was confirmed by measuring the increased release of osteoclast marker tartrate resistant acid phosphatase (TRAP), suggesting that osteoclasts were actively resorbing mineralised tissue. Resorption pits were visualised using scanning electron microscopy. Mineralised matrix formation and resorption were quantified using μCT and subsequent scans were registered to visualise remodelling. Both formation and resorption occurred in parallel in the co-culture. The resorbed tissue volume exceeded the formed tissue volume after day 12. In conclusion, the current model was able to visualise, localise and quantify mineralised matrix formation and resorption. Such a model could be used to facilitate fundamental research on bone remodeling, facilitate drug testing and may have clinical implications in personalised medicine by allowing the use of patient cells.

Keywords: Osteoclasts, osteoblasts, co-culture, scaffolds, mineralisation, bioresorption, bioreactors, bone.

***Address for correspondence**: Dr Sandra Hofmann, Eindhoven University of Technology, PO Box 513, 5600 MB Eindhoven, the Netherlands.
Telephone number: +31 402473494 Email: S.Hofmann@tue.nl

List of abbreviations

ANOVA	analysis of variance
bFGF	basic fibroblast growth factor
CTDI	computed tomography dose index
FBS	foetal bovine serum
H&E	haematoxylin and eosin
HFIP	1,1,1,3,3,3-hexafluoro-2-propanol
HMDS	1,1,1-trimethyl-N-(trimethylsilyl) silanamine
hMSC	human mesenchymal stromal cells
IHC	immunohistochemistry
M-CSF	macrophage colony-stimulating factor
NEAA	non-essential amino acids
P/S	penicillin/streptomycin
PBS	phosphate buffered saline
pNPP	(4-nitrophenyl) dihydrogen phosphate
RANKL	receptor activator of nuclear factor kappa-B ligand
RT	room temperature
SD	standard deviation
SEM	scanning electron microscopy
SF	silk fibroin
TRAP	tartrate resistant acid phosphatase
UPW	ultra-pure water
μCT	micro-computed tomography

Introduction

Bone consists of three main cell types: bone-forming osteoblasts, bone-resorbing osteoclasts, and regulating osteocytes. As the mechanical demands placed upon bones change, bones adapt their structure by removing obsolete material or producing new material where it is needed to provide the required strength. This process is made possible by the organisation of osteoblasts and osteoclasts into local bone remodelling teams called basic multicellular units (Frost, 1969). While the exact inter- and intracellular mechanisms underlying bone remodelling and bone diseases have not been completely elucidated, many factors and cytokines that play a role in these processes have been identified (Deschaseaux *et al*., 2010; Matsuo and Irie, 2008; Sims and Gooi, 2008), and are being targeted by treatment options for diseases such as osteoporosis (Bellido, 2014; Matsuo and Irie, 2008). Unfortunately, even with access to various forms of treatment, it is not yet possible to reverse the degenerative nature of osteoporosis, but merely to slow down the progression. In order to elucidate the cellular and molecular mechanisms underlying bone remodelling, as well as to facilitate the development of new and personalised treatments for bone diseases, accurate, reproducible and translatable model systems are needed.

Animal models are considered a fundamental part of preclinical research, but using animals raises ethical concerns and is generally more time-consuming and expensive than *in vitro* research. Although human health and disease are the objects of interest, animals with a similar yet still different physiology are being used, which can lead to poor translation of results from pre-clinical animal studies to human clinical trials, and the failure of highly promising discoveries to enter routine clinical use (Burkhardt and Zlotnik, 2013; Contopoulos-Ioannidis *et al*., 2003). Those limitations and the desire to reduce, refine and replace animal experiments gave rise to the development of *in vitro* models.

In vitro bone models come with both advantages and limitations. While animal cells are easily accessible and easy to work with, they can respond differently from human cells (Jemnitz *et al*., 2008). *In vitro* models have the advantage that they can make use of human cells. Many *in vitro* experiments are conducted in 2D monolayer (Amizuka *et al*., 1997; Marino *et al*., 2014), which is suitable for the research questions they address. However, *in vivo* bone remodelling occurs in a 3D environment where cells can deposit and resorb quantifiable volumes of mineralised tissue, and where cells likely respond differently from in 2D (Edmondson *et al*., 2014; Li and Kilian, 2015). Ideally, to study human bone remodelling and quantify bone formation or resorption *in vitro*, primary human cells should be cultured in a 3D environment (Owen and Reilly, 2018). As bone formation and resorption occur simultaneously, a co-culture of both osteoblasts and osteoclasts is required, in particular because it is known that these cells are capable of interacting with each other through paracrine signalling (Matsuo and Irie, 2008). There are various methods to co-culture cells (Goers *et al*., 2014; Paschos *et al*., 2015; Zhu *et al*., 2018), but only a direct co-culture within the same construct allows a two-way exchange of signalling molecules and access to the same mineralised surface. Functionality of the cells could then be assessed by quantification of the net effect of stimuli on remodelling, as well as the individual effects of resorption and formation.

Recently, 3D osteoclast models (Heinemann *et al*., 2010; Kleinhans *et al*., 2015; Perrotti *et al*., 2009) and 3D osteoblast-osteoclast co-culture models (Hayden *et al*., 2014; Papadimitropoulos *et al*., 2011) have been designed to specifically study 3D bone resorption or remodelling using a variety of end-point techniques such as histological imaging, electron microscopy, surface metrology, polymerase chain reaction and various cell marker assays. These studies provided first insights into human bone remodelling but should be improved by quantitatively monitoring bone remodelling over time. Registration of consecutive images similarly to *in vivo* bone studies in mice (Hagenmüller *et al*., 2007; Schulte *et al*., 2011a; Schulte *et al*., 2011b) would allow assessing both formation and resorption in parallel, and thereafter separating the contribution of osteoblasts from those of osteoclasts.

The aim of the present study was to establish a 3D co-culture of primary human osteoblasts and osteoclasts on silk fibroin (SF) scaffolds in which 1) osteoblasts first deposit a mineralised bone-like matrix, 2) monocytes are differentiated into resorbing osteoclasts, and 3) the mineralised matrix formation by osteoblasts and the resorption by osteoclasts can be both monitored over time. Such a human *in vitro* model would allow the localisation and quantification of formation and resorption events over time to provide a powerful tool for fundamental research on osteoblast-osteoclast interaction and bone remodelling and could have implications for drug development and personalised medicine.

Materials and Methods

Materials

Dulbecco's modified Eagle medium (DMEM Cat. No 41966) and non-essential amino acids (NEAA) were from Life Technologies (Bleiswijk, the Netherlands). Foetal Bovine Serum (FBS, batch F7524-500ML / lot BCBV7611) was from Sigma Aldrich / Merck. Antigen retrieval citrate buffer, RPMI-1640 medium, poly-L-lysine coated microscope slides and SnakeSkin Dialysis tubing were from Thermo Fisher Scientific (Breda, the Netherlands). Disposable biopsy punches were from Amstel Medical (Amstelveen, the Netherlands) Trypsin-EDTA (0.25 %) and penicillin/streptomycin (P/S) were from Lonza (Breda, the

Netherlands). Human bone marrow (healthy male subject, 24 years old) was from Lonza (Walkersville, MD, USA). The human buffy coat was from Sanquin (Nijmegen, the Netherlands). Lymphoprep™ was from Axis-Shield (Oslo, Norway). MACS® Pan Monocyte Isolation Kit was from Miltenyi Biotec (Leiden, the Netherlands). Recombinant human basic fibroblast growth factor (bFGF), macrophage colony stimulating factor (M-CSF) and receptor activator of nuclear factor kappa-B ligand (RANKL) were from PeproTech (Rocky Hill, NJ, USA). *Bombyx mori L.* Silkworm cocoons were from Tajima Shoji Co., LTD. (Yokohama, Japan). Thin bleach was from the local grocery store. All other substances were of analytical or pharmaceutical grade and obtained from Sigma Aldrich / Merck (Zwijndrecht, the Netherlands).

Methods

Silk fibroin scaffold fabrication

Silk fibroin (SF) scaffolds were produced as previously described (Meinel *et al.*, 2005; Melke *et al.*, 2018; Nazarov *et al.*, 2004). *Bombyx mori L.* silkworm cocoons were degummed by boiling in 0.2 mol/L Na_2CO_3 in ultra-pure water (UPW) twice for 1 h, rinsed in boiling UPW followed by 10 × washing in cold UPW. The silk was left to dry overnight and was dissolved in 9 mol/L LiBr in UPW (10 % w/v) at 55 °C for 1 h, cooled to RT and filtered through a 5 µm filter. Then, the silk solution was dialysed against UPW for 36 h using SnakeSkin Dialysis Tubing (molecular weight cut-off: 3.5 kDa). UPW was replaced after 1, 3, 12, 24 and 36 h. Dialysed silk solution was frozen at − 80 °C, lyophilised (Freezone 2.5, Labconco, Kansas City, MO, USA) for 4 d and dissolved to a 17 % (w/v) solution in 1,1,1,3,3,3-hexafluoro-2-propanol (HFIP). 1 mL silk-HFIP solution was added to 2.5 g NaCl with an average granule size between 250 and 300 µm in a Teflon container and allowed to dry at RT for 4 d. Silk-salt blocks were immersed in 90 % (v/v) methanol in UPW for 30 min to induce β-sheet formation (Tsukada *et al.*, 1994) and dried at RT overnight. Silk-salt blocks were mounted in a precision cut-off machine (Accutom-5®, Struers GmbH Nederland, Maassluis, the Netherlands), and cut into discs of 3 mm height. NaCl was leached out in UPW for 2 d. UPW was replaced after 2 h, and then 2 × per day. Scaffolds were punched with a 5 mm diameter disposable biopsy punch and sterilised by autoclaving in phosphate buffered saline (PBS) at 121 °C for 20 min.

hMSC expansion, seeding onto scaffolds and osteoblastic differentiation

This study used human mesenchymal stromal cells (hMSC) at passage 5 that were isolated from human bone marrow (healthy male subject, 24 years of age) and characterised in a previous study (Hofmann *et al.*, 2007). Cells were thawed, seeded at 2.5×10^3 cells/cm² and expanded for 6 d in control medium (DMEM, 10 % FBS, 1 % P/S) supplemented with 1 % NEAA and 1 ng/L bFGF. Scaffolds pre-wetted in control medium were seeded with 1 million hMSCs each in 20 µL control medium and incubated for 90 min at 37 °C. The constructs were then transferred to 4 custom-made spinner flask bioreactors ($n = 4$ *per* bioreactor) as described previously (Melke *et al.*, 2018). Each bioreactor contained a magnetic stir bar and was placed on a magnetic stirrer plate (300 rpm, RTv5, IKA, Germany) in an incubator (37 °C, 5 % CO_2). Each bioreactor was filled with 5 mL osteogenic medium (control medium supplemented with 50 µg/mL L-ascorbic-acid-2-phosphate, 1×10^{-7} mol/L dexamethasone, 0.01 mol/L β-glycerophosphate) and medium was changed 3 times a week for 13 weeks. In this study the 3D monoculture of hMSCs on SF scaffolds, differentiation into osteoblasts and matrix formation was designated as '3D osteoblast culture'.

Monocyte isolation from peripheral blood

A human peripheral blood buffy coat from a healthy anonymous volunteer who gave informed consent was obtained from the local blood donation centre (Sanquin, Nijmegen, the Netherlands). The buffy coats (~ 50 mL) was diluted to 180 mL in 0.6 % (w/v) sodium citrate in PBS adjusted to pH 7.2 at 4 °C (Citrate-PBS), after which the peripheral mononuclear cell fraction was isolated by carefully layering 30 mL diluted buffy coat onto 16 mL Lymphoprep™ iso-osmotic medium in 6 separate 50 mL centrifugal tubes, and centrifuging for 30 min with lowest brake and acceleration at 800 ×*g* at RT, as described previously (Bonito *et al.*, 2018). Mononuclear cells were layered on top of the iso-osmotic layer and were transferred to new tubes using a sterile Pasteur pipette. Isolated cells were washed (suspended in 50 mL Citrate-PBS and centrifuged for 10 min at 350 ×*g*) 5 × to remove all Lymphoprep™, diluted in freezing medium 1 (20 % FBS in RPMI-1640) and aliquoted into cryovials, 50 million cells in 750 µL *per* vial. Into each cryovial 750 µL freezing medium 2 (20 % dimethyl sulphoxide in freezing medium 1) was added and the cryovials were transferred to Nalgene® freezing containers overnight (− 80 °C), before being transferred to liquid nitrogen tanks for long-term storage. Cells were taken out of liquid nitrogen and rapidly thawed before use without passaging. A purified monocyte fraction was isolated from the mononuclear cells using the negative selection MACS® Pan Monocyte Isolation Kit (Miltenyi Biotec) with LS columns according to the manufacturers' instructions. After magnetic separation, the cells were centrifuged for 10 min at 350 ×*g*, resuspended in osteoclast control medium (RPMI-1640, 10 % FBS, 1 % P/S) and counted. The purified monocyte fraction will from now on be referred to as 'monocytes'.

2D osteoclast monoculture

A 2D culture was conducted to show the differentiation potential of the monocytes and the resorption potential of the osteoclasts. To verify that the monocytes could form multinucleated TRAP expressing and resorbing osteoclast-like cells, 0.25×10^6 monocytes *per* cm² ($n = 4$ *per* time point)

were seeded in priming medium (osteoclast control medium + 50 ng/mL M-CSF) on 24-well Corning® Osteo Assay plates and regular tissue culture plastic 24-well tissue culture plates in monolayer (without scaffolds). Priming medium was replaced with osteoclastogenic medium (priming medium + 50 ng/mL RANKL) after 48 h. Osteoclastogenic medium was replaced 3 × per week for up to 19 d. This experiment was designated as '2D osteoclast monoculture'.

2D resorption assay

The Corning® Osteo Assay plate from the 2D osteoclast monoculture was analysed for resorption according to the manufacturers' instructions. Cells were removed by incubation in 5 % bleach for 5 min, and their removal was confirmed with light microscopy. The plate was incubated with 5 % (w/v) aqueous silver nitrate for 30 min at RT in the dark, washed with UPW for 5 min, followed by 5 % (w/v) sodium carbonate in neutral buffered formalin for 4 min. The plate was dried at 50 °C for 1 h. Bright field images were taken with a Zeiss Axio Observer Z1 microscope.

Seeding monocytes onto tissue-engineered (pre-mineralised) constructs

Constructs which had been in culture for 13 weeks (3D osteoblast culture) were incised to allow monocyte seeding to the centre of the constructs. An incision of approximately 4 mm deep was made into the constructs at 1.5 mm height in the transverse plane, allowing the construct to fold partly open. Constructs were submersed for 1 h in priming medium. 1 million monocytes in 7.5 µL priming medium were seeded into the incision of the constructs and incubated for 180 min at 37 °C to allow the cells to attach. The constructs were then placed back into the bioreactors ($n = 4$ *per* bioreactor, one bioreactor *per* time point for histology and SEM, and one bioreactor that was scanned using µCT for the duration of the study). Each bioreactor was filled with 5 mL priming medium, resulting in 1.25 mL of medium *per* construct. No stirring was applied. The 3D co-culture of osteoblasts with monocytes was designated as '3D co-culture'. Priming medium was replaced with osteoclastogenic medium (priming medium + 50 ng/mL RANKL) after 48 h (De Vries *et al*., 2015). Osteoclastogenic medium was replaced 3 × *per* week for up to 22 d. Constructs were sacrificed at day 12, 18 and 25 for SEM, histology and immunohistochemistry. One bioreactor was used for µCT imaging of the co-culture.

µCT imaging

µCT measurements were performed on a µCT100 imaging system (Scanco Medical, Brüttisellen, Switzerland) after 3, 4, 5 and 13 weeks of 3D osteoblast culture to monitor tissue mineralisation. After 13 weeks, monocytes were seeded into the (now incised) constructs, and were scanned again after 4, 12 and 22 d of 3D co-culture to monitor mineralised tissue resorption. Scanning was performed at an isotropic nominal resolution of 17.2 µm, energy level was set to 45 kVp, intensity to 200 µA, 300 ms integration time and two-fold frame averaging, resulting in a computed tomography dose index (CTDI) in air of 230 mGy. A constrained Gaussian filter was applied to reduce part of the noise. Filter support was set to 1.0 and filter width sigma to 0.8 voxel. For all but the last 2 scans, a region of interest of 205 slices was selected within the bioreactor insert. This allowed to always scan the same regions of every scaffold and to limit the required scan time and thus x-ray exposure of the cells to 30 min per construct. For the last 2 scans, the whole construct was scanned to facilitate 3D registration, with a scan time of approximately 60 min *per* construct. Filtered greyscale images were segmented at a global threshold of 23 % of the maximal greyscale value and processed using image processing language (IPLFE v2.03, Scanco Medical AG) available on the PC supplied with the scanner. Unconnected objects smaller than 50 voxels were removed by component labelling (function: cl_nr_extract, min_number 50) and neglected for further analysis. Quantitative morphometry was performed using a Triangulation Metric Gobj DA Procedure (function: tri_da_metric, default settings) to assess the mineralised tissue volume of a region of interest of 205 slices *per* construct. 3D osteoblast culture quantitative µCT data was used as such, whereas 3D co-culture quantitative µCT data was transformed in such a way that the mineralised volumes of the first scan of each individual construct (day 4 of co-culture) was set to 100 %, and all successive scans were presented as percentages of change with respect to the first scan. Rigid 3D registration was used to register the follow-up to the baseline image (images of day 22 and 12 respectively of the 3D co-culture) of the complete scans of the constructs (Ellouz *et al*., 2014). After registration, colour coding was used to label voxels only present at day 12 in blue (resorption), voxels only present at day 22 in orange (formation), and voxels present in both images in grey-purple (unaltered). Unconnected objects smaller than 50 voxels were removed as before. The number of voxels for each colour was extracted by creating a histogram of all corresponding values (function: histo, screentab on, range from 0 to 123). Unaltered and resorbed voxels added together were used as 100 % baseline reference for each construct. Resorption, formation and unaltered volumes were expressed as percentage of the baseline. Background voxels were omitted from further analysis. All images shown are from component-labelled scans.

Histology

Constructs for histology and immunofluorescence were fixed in 10 % neutral buffered formalin for 24 h at 4 °C, dehydrated and embedded in paraffin wax (70, 80 and 96 % EtOH for 1.5 h each, 3 × 100 % EtOH for 1 h each, 2 × xylene for 1.5 h each, 2 × paraffin wax for 2 h each), sectioned vertically and cut into

10 μm thick sections and mounted on poly-L-lysine coated microscope slides. Sections were dewaxed and rehydrated (2 × 5 min xylene, 3 × 100 %, 1 × 96 %, 70 % and 0 % EtOH in UPW for 2 min each). For overview, sections were stained with haematoxylin and eosin (H&E) (10 min Mayer's haematoxylin, 1 min acidified tap water, 5 min running tap water, 3 min Eosin Y, 1 min running tap water). To visualise mineralised tissue, sections were stained with von Kossa (30 min in 1 % aqueous silver nitrate (w/v) under UV light, rinsed with UPW, 5 min in 5 % sodium thiosulphate (w/v), rinsed with UPW, 5 min in nuclear fast red, rinsed in UPW). Stained sections were dehydrated (10 dips in 70 %, 90 % and 3 × 10 dips in 100 % EtOH in UPW, 2 × 3 min xylene) and coverslipped with Entallan®.

Immunofluorescence

Sections were dewaxed and rehydrated as described before. Antigen retrieval was done on paraffin wax sections with citrate buffer at 95 °C for 20 min and left to cool back to RT. Cross-reactions were reduced by blocking with 10 % donkey serum for 30 min. Primary antibodies were diluted in PBS and incubated at 4 °C overnight. Sections were rinsed in PBS and incubated with secondary antibodies at RT for 1 h. Sections were labelled with DAPI for cell nuclei and with antibodies for osteoblast marker osterix, osteocyte marker sclerostin and osteoclast marker integrin β3 (CD61), which was chosen in favour of TRAP because of its specificity towards differentiated osteoclasts, while TRAP is present in osteoclast-like cells as well (Barbeck *et al.*, 2017; Nakamura *et al.*, 2007). The 2D osteoclast monoculture in plastic well-plates was immunofluorescently labelled for osteoclast marker TRAP, with TRITC-conjugated-Phalloidin to stain the actin cytoskeleton, and DAPI for cell nuclei to study multinucleation. Stained wells were imaged with a layer of PBS on top with the Zeiss Axiovert 200M microscope, and sections were coverslipped with Mowiol® and imaged with the Leica TCS SP5X microscope. Antibodies are listed in Table 1.

SEM

Constructs for SEM were fixed at day 12 and 18 in 2.5 % glutaraldehyde for 24 h at 4 °C, dehydrated with a graded ethanol series (2 × 50 %, 70 % and 95 %, 3 × 100 % 10-15 min each) followed by a graded 1,1,1-Trimethyl-N-(trimethylsilyl)silanamine (HMDS)/ethanol series (1 : 2, 1 : 1, 2 : 1, 3 × 100 % HMDS 15 min each), dried at RT overnight and sputter coated with 5 nm gold (Q300TD, Quorum Technologies Ltd, Laughton, UK) prior to imaging with SEM (Quanta600, FEI Company, Eindhoven, the Netherlands) with spot size 3.0, 5.00 kV, working distance 10 mm).

TRAP quantification in supernatant

Supernatant medium samples were taken and stored at − 80 °C at each medium change during the 3D co-culture (n = 4 *per* bioreactor) and the entire 2D osteoclast monoculture (n = 4 *per* group). 100 μL pNPP buffer (1 mg/mL para-nitrophenylphosphate (pNPP), 0.1 mol/L sodium acetate, 0.1 % (v/v) triton-X-100 in PBS, first adjusted to pH 5.5, then supplemented with 30 μL/mL tartrate solution (Sigma Aldrich)) and 20 μL culture medium or nitrophenol standard in PBS were incubated in translucent 96-well plates at 37 °C. After 90 min, 100 μL 0.3 mol/L NaOH was added to stop the reaction. Absorbance was read at 405 nm to obtain TRAP enzyme activity. The resulting values were transformed to amount of transformed pNPP *per* min.

Statistical analysis

Quantitative data is represented as average ± SD. Statistical analysis was performed using SPSS version 26 (IBM Corp, Armonk, NY, USA). Time points and groups that were statistically compared were tested for normality using the Shapiro-Wilk normality test, and were normally distributed. Homogeneity of variance was assessed with the Levene's test for equality of variances. A repeated measures analysis of variances (ANOVA) was performed on the 3 consecutive scans with 205 slices each of the 3D co-culture. Paired-samples t-tests were used to compare total volume change between day 12 and 22 of the complete μCT scans, and the difference between quantified formation and resorption data. A one-way ANOVA with *post-hoc* Bonferroni correction for multiple comparisons was used to compare differences between both culture surfaces and all relevant time points of the TRAP activity of cells seeded in 2D on plastic or Osteo Assay plates. Differences were considered statistically significant at a level of $p < 0.05$.

Table 1. Antibodies used for immunofluorescence

Antigen	Supplier	Cat. No	Conjugate	Species	Dilution
Osterix	Abcam	Ab22552	-	Rabbit	1 : 200
Sclerostin	ThermoFisher	PA5-37943	-	Goat	1 : 200
Integrin β3	Biorbyt	Orb248939	-	Mouse	1 : 100
TRAP	Santa-Cruz	Sc-30833	-	Goat	1 : 100
Anti-mouse IgG (H+L)	Jackson	715-545-150	Alexa488	Donkey	1 : 300
Anti-rabbit IgG (H+L)	Jackson	711-605-152	Alexa647	Donkey	1 : 300
Anti-goat IgG (H+L)	Invitrogen	A21432	Alexa555	Donkey	1 : 300
Anti-goat IgG (H+L)	Molecular Probes	A11055	Alexa488	Donkey	1 : 300

Results

hMSCs differentiate into osteoblasts and form mineralised tissue

hMSCs were seeded onto SF scaffolds and differentiated into mineralised matrix depositing osteoblasts for 13 weeks. Starting from week 3, mineralised matrix formation was monitored with consecutive µCT scans. Non-mineralised SF scaffolds were not visible on µCT images. Mineralisation became detectable from week 4 onwards, and mineralisation continued until week 13 (Fig. 1**a**). Mineralised volume increased over time to 17.62 ± 4.69 mm^3 at week 13 (Fig. 1**b**). A cross-section revealed that mineralised tissue was present throughout the construct (Fig. 1**c**). Tissue formation on the outside of the construct completely concealed the original porous architecture, which would have prevented cells seeded on top to penetrate into the construct and necessitated incising the construct to seed cells inside for the co-culture (Fig. 1**d**). An SEM image of an empty scaffold without any seeded cells is provided to illustrate the effect of osteoblastic tissue formation on the geometry of the construct (Fig. 1**e**).

Monocytes differentiate into resorbing TRAP expressing multinucleated osteoclasts in 2D

To verify that the primary monocytes were capable of differentiating into TRAP expressing, resorbing, multinucleated osteoclasts, monocytes were seeded in 2D on tissue culture plastic and on Osteo Assay plates to visualise resorption. On the plastic surface, multinucleated cells with more than 3 nuclei that express osteoclast marker TRAP with a well-defined actin cytoskeleton were seen (Fig. 2**a**, image of day 12), indicating that they differentiated into osteoclast-like cells. During the differentiation from monocytes to osteoclasts, TRAP release increased until approximately day 12. Interestingly, cells cultured on Osteo Assay plates continued to release TRAP throughout the culture period, whereas cells cultured on plastic showed a rapid decrease in TRAP release over time after day 12 (Fig. 2**b**). The highest peak TRAP activities were 16.62 ± 0.92 µmol/L pNPP / min / well at day 14 on the Osteo Assay surface and 14.88 ± 0.64 µmol/L pNPP / min / well at day 12 on tissue culture plastic, but the difference was not statistically significant ($p = 0.173$). TRAP activity curves started to significantly deviate from each other from day 14 onward ($p < 0.001$). Cells were able to resorb parts of the mineralised layer (in black) creating resorption trails (in white) on Osteo Assay plates (Fig. 2**c**). At the first time point for the resorption assay (day 8), resorption was already visible. On later time points, more resorption was seen.

Monocytes differentiate into resorbing TRAP expressing osteoclasts in 3D

Once a mineralised matrix was deposited by osteoblasts, monocytes were seeded into the centre of the construct by creating a transverse incision through the mineralised construct. The culturing environment was switched from an osteogenic

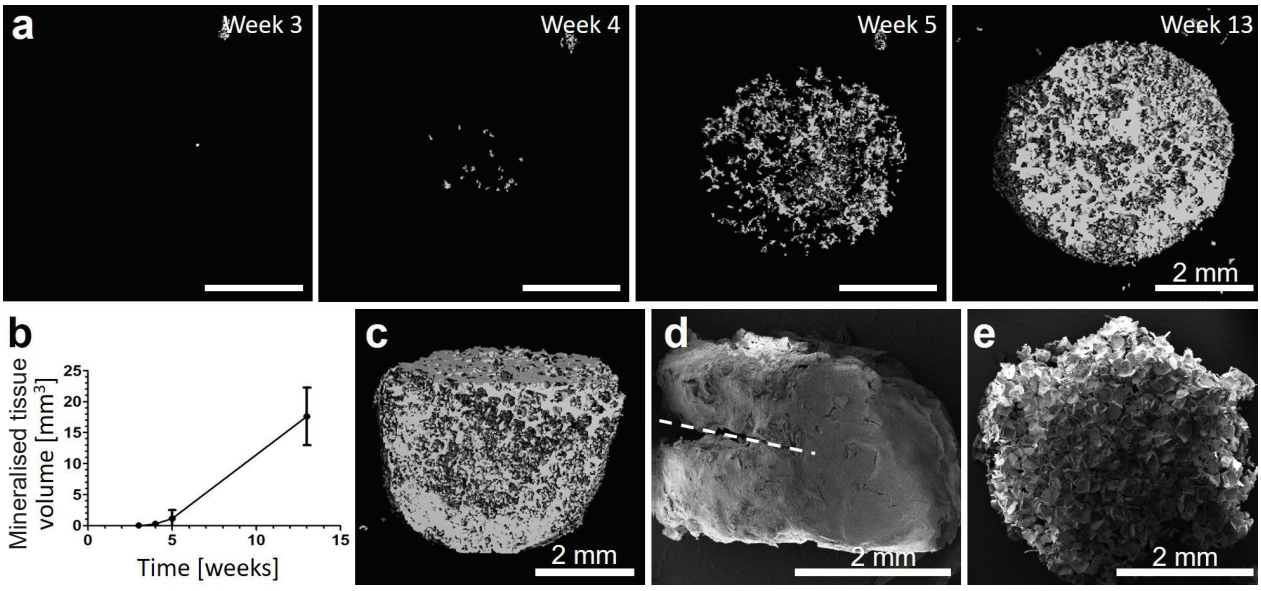

Fig. 1. Formation of a mineralised matrix by osteoblasts on 3D SF scaffolds. (**a**) Non-mineralised SF scaffolds are not visible on µCT images. Mineralised matrix became detectable after 4 weeks of culture and increased in volume over time. Images are top-down views. Scale bars are 2 mm. (**b**) The mineralised tissue volume of the constructs continuously increased over time. (**c**) An inclined view on a digital cross-section of a µCT image shows the mineralised matrix distribution within a construct at week 13. (**d**) SEM example image of an SF scaffold after 9 weeks of osteoblast culture, showing that tissue formation completely concealed the pores of the SF scaffold, necessitating incising the construct to seed monocytes inside. A dashed line shows where the construct was incised for seeding. (**e**) SEM control image of an SF scaffold without any cells.

medium with mechanical stimulation using a spinner flask bioreactor to a static environment with a medium inducing monocyte differentiation towards osteoclasts. The presence of resorbing osteoclast-like cells on the constructs was verified with SEM. Osteoclast-like cells were identified based on their size (> 50 μm in diameter) (Fig. 3**a**,**b**) and their proximity to what could be small resorption pits (Fig. 3**a**). The immediate surrounding area of the pits in Fig. 3**a** seemed morphologically different from the area surrounding it. Neither pits nor such areas were found on control constructs without seeded monocytes (Fig. 3**c**). Images of unseeded SF scaffolds illustrate the architecture of these scaffolds prior to the experiment (Fig. 3**d**,**e**). TRAP analysis in the supernatant showed an increasing release until day 12, followed by a continuous release of TRAP until the end of culture (Fig. 3**f**).

Histology confirms the presence of bone cells and mineralised matrix in 3D co-culture

Constructs for histological images were collected at day 12 to avoid a time point towards the end of the expected life expectancy of osteoclasts. The presence of cells throughout the construct was confirmed with H&E (Fig. 4**a**,**d**). Deposition of a mineralised matrix throughout the construct volume was confirmed with von Kossa staining (Fig. 4**b**,**e**) and has supported the threshold choice for the μ-CT analysis. The transverse incision for seeding monocytes can be seen in the histological images. The presence of osteoblast-like-, osteoclast-like- and osteocyte-like cells was confirmed with fluorescent staining of markers typical for the respective cell type (osterix, integrin β3 and sclerostin, respectively) (Fig. 4**c**,**f**,**g**-**j**). Osteoblast- and osteocyte-like cells were abundantly found throughout the construct, whereas only few integrin β3-positive osteoclast-like cells were detected. Classical morphological features of the cells could not be visualised as a result of creating 2D sections of a 3D tissue, where the odds of a cell lying precisely within the cutting plate are slim.

Formation and resorption of mineralised tissue were quantified in 3D co-culture

During the 3D osteoblast-osteoclast co-culture, the constructs were subjected to 3 additional successive μCT scans to monitor both mineralised tissue formation and resorption in parallel. The registration of the consecutive scans from day 12

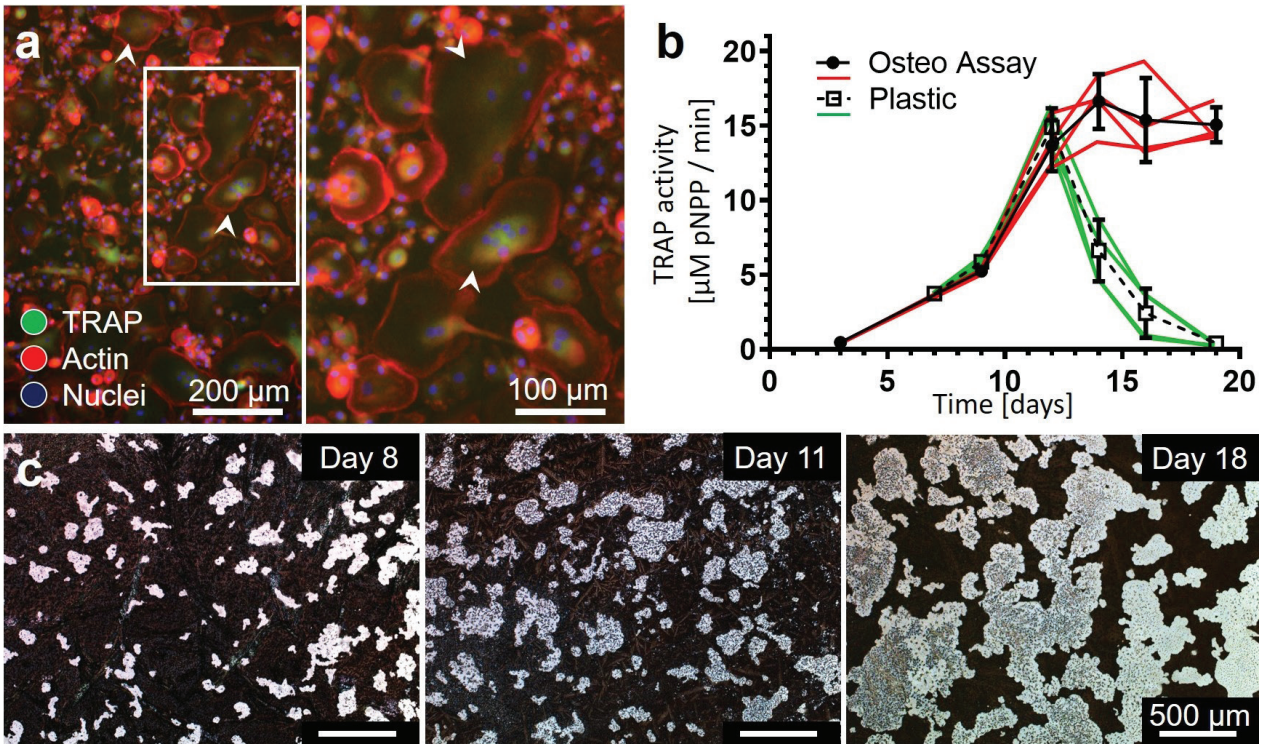

Fig. 2. 2D verification of the capability of monocytes to differentiate into functional osteoclast-like cells. (**a**) After a 12 d 2D culture on tissue culture plastic, TRAP-positive (green) multinucleated (blue) cells with a clearly defined actin cytoskeleton (red) could be distinguished. A magnified image is shown to verify the presence of multinucleated TRAP-positive cells, two of which are marked with white arrowheads in both the complete image and magnified panel. (**b**) TRAP release into the medium increased until approximately day 12, and was dependent on the surface. On a resorbable surface (Osteo Assay plate, average activity indicated by black line and circles, and individual samples as red lines), TRAP was expressed longer than on tissue culture plastic (average activity indicated by dotted line and hollow squares, individual lines in green). (**c**) The cells were capable of resorbing a resorbable surface, and the resorbed area increased over time. Unresorbed surfaces are stained black, whereas resorption trails are white (transparent).

and 22 after co-culture initiation revealed that both resorption (blue) and formation (orange) occurred in parallel throughout the construct volumes (Fig. 5**a**) Constructs were digitally sliced in halves to reveal the inside. Large areas coloured grey-purple indicate volumes that remained unchanged between scans. On the surfaces of the grey areas many resorption and formation events have taken place. The mineralised volume of the constructs increased on average by 8.35 ± 3.85 % ($p = 0.023$) from day 4 to 12 of the 3D co-culture (Fig. 5**b**). This confirmed that osteoblasts were continuing to deposit mineralised matrix although they were not in their preferred environment anymore, while the monocytes likely had not yet reached their functional osteoclastic state. From day 12 to 22, the total mineralised volume decreased on average by 7.19 ± 0.99 % ($p = 0.001$). This indicates a switch from mainly osteoblastic formation to mainly osteoclastic resorption of mineralised tissue in this period. Nevertheless, although there was overall a net resorptive effect, the formation of tissue still continued but was significantly lower ($p = 0.0017$) than the resorption (21.16 ± 1.18 % *versus* 29.06 ± 2.68 %, respectively) (Fig. 5**c**).

Discussion

The aim of this study was to establish a 3D co-culture in which the formation of a mineralised extracellular matrix by osteoblasts and its resorption by osteoclasts could be localised, visualised and quantified after the application of the corresponding biochemical cues. A 3D *in vitro* co-culture system comprising human cells was created in which osteoblasts seeded onto SF scaffolds formed a mineralised matrix and osteoclasts resorbed the mineralised tissue when exposed to the correct environmental conditions. With µCT monitoring, the simultaneous formation and resorption process could be localised, quantified, and monitored. Cells performed as anticipated when stimulated with their corresponding biochemical cues. Osteoclasts were active for longer than expected when cultured on resorbable surfaces. While cell interaction was most likely occurring in parallel, the artificial environment with selected biochemical cues imposed on them was sufficient to steer the processes of formation and resorption into the desired direction.

hMSCs differentiated towards osteoblasts, deposited a mineralised matrix over time in monoculture, and continued to deposit mineralised

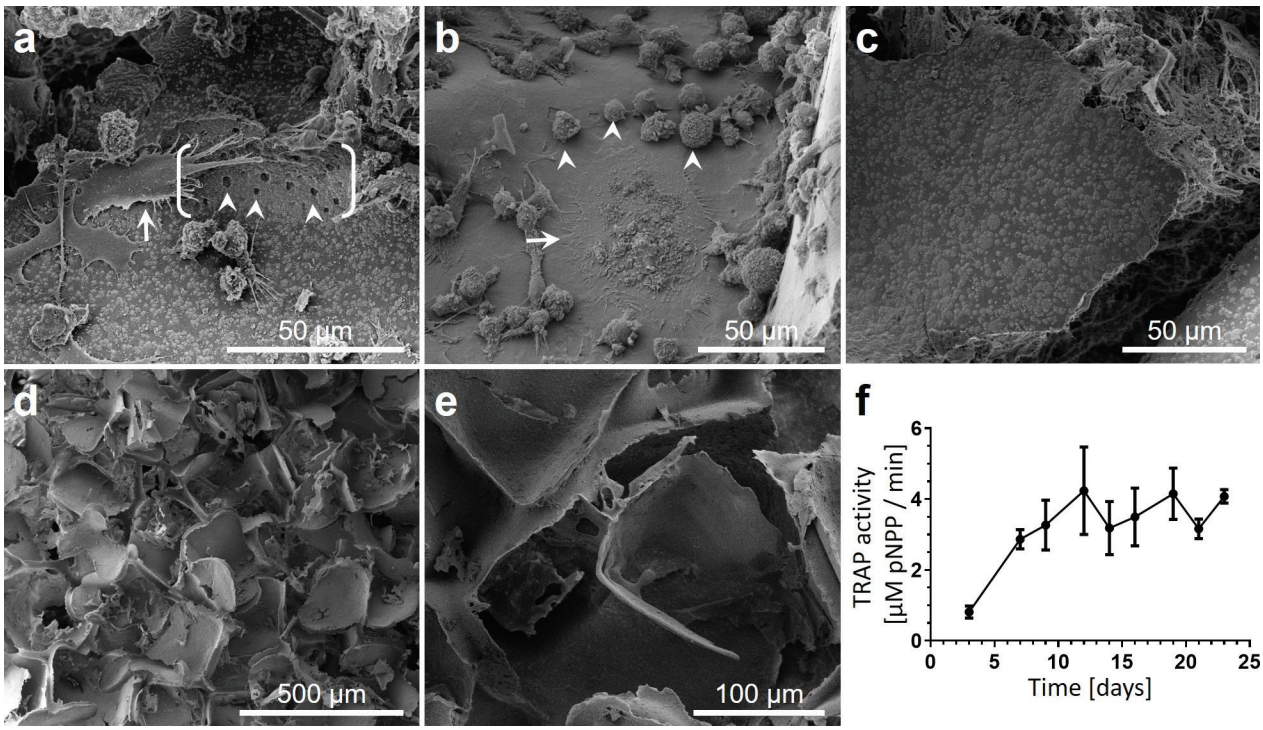

Fig. 3. Osteoclasts created resorption pits and released TRAP on tissue-engineered 3D constructs. (**a**) SEM image at day 12 of the 3D co-culture showing an osteoclast (arrow) and a series of pits (arrowheads, not all pits are marked) on the mineralised matrix. The surface in close proximity to the pits (within brackets) is morphologically different from the surrounding surface, suggesting the presence of a larger but flatter resorbed surface area, possibly an osteoclast trail. (**b**) SEM image at day 12 of the co-culture showing a flat osteoclast (arrow) and several round and smaller cells, possibly monocytes based on their size and morphology (arrowheads, not all cells are marked). (**c**) SEM image of a mineralised construct where no monocytes were seeded. (**d** and **e**) low and high magnification SEM images of an empty SF scaffold prior to seeding MSCs. (**f**) TRAP release in the 3D co-culture increased until approximately day 12 after the seeding of monocytes. From then on, TRAP activity stayed high until the end of the co-culture (day 23).

matrix in co-culture. Matrix deposition was monitored with μCT, in a manner similar to what others have shown (Hagenmüller *et al.*, 2007; Hofmann *et al.*, 2013; Melke *et al.*, 2018). Matrix deposition continued throughout the co-culture with monocytes, even after the medium was switched from osteogenic medium to osteoclastogenic medium and mechanical loading was stopped. While it has been shown previously that mechanical loading can promote mineralised matrix deposition both *in vivo* and *in vitro* (Klein-Nulend *et al.*, 2012; Klein-Nulend *et al.*, 2013; Melke *et al.*, 2018) an environment high in fluid flow does not represent the physiological environment of monocyte recruitment, attachment and differentiation into osteoclasts (Klein-Nulend *et al.*, 2012; Kulkarni *et al.*, 2012; Pathak *et al.*, 2015). The continued mineralised matrix formation after the initiation of the co-culture until approximately day 12 could indicate that osteoblasts, once activated with the correct mechanical or biochemical stimuli, continue to deposit mineralised matrix even after these stimuli have been removed. This could occur as a result of factors liberated from the matrix or expressed by the newly seeded monocytes that are now differentiating towards osteoclasts (Pang *et al.*, 2013; Tang *et al.*, 2009; Xian *et al.*, 2012). Alternatively, osteoblasts could be responsible for the creation of the collagen framework and biochemical environment necessary for mineralisation, but not required for the subsequent mineralisation thereof (Samal *et al.*, 2014). Between day 12 and 22 of co-culture, the overall mineralised tissue volume decreased and the overall remodelling balance switched from mainly formation to mainly resorption. The registration of consecutive scans allowed localising and visualising that both formation and resorption processes were present between day 12 and 22 of co-culture, confirming that they occurred in parallel.

A mineralised surface seems to prolong osteoclast activity beyond their expected lifespan of approximately 2 weeks (Owen and Reilly, 2018; Parfitt, 1994). Osteoclast activity was determined by measuring TRAP, a proteolytic enzyme secreted predominantly by osteoclasts which plays a role in

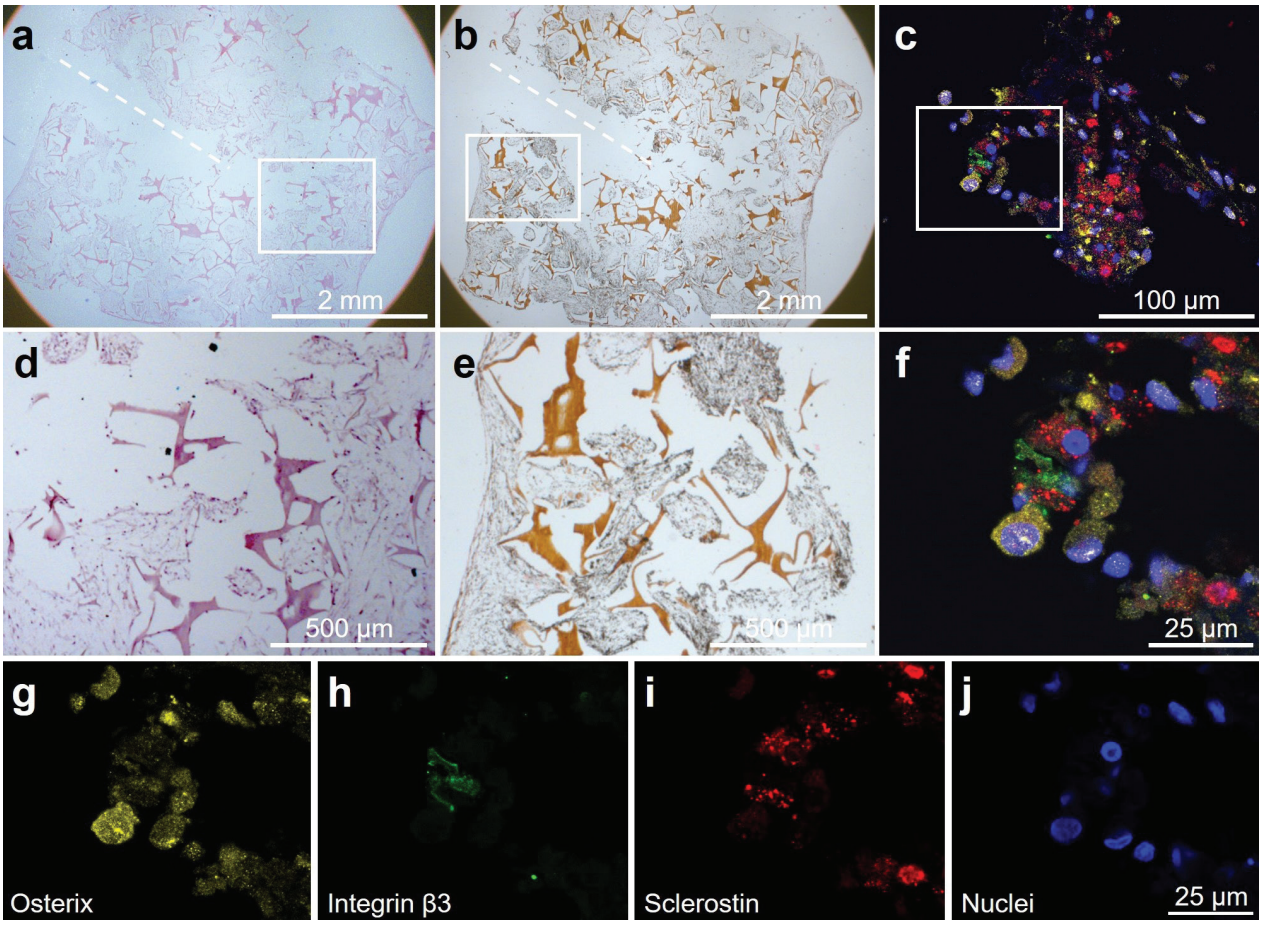

Fig. 4. Cells expressing typical markers for osteoblasts, osteoclasts and osteocytes were present at day 12 of 3D osteoblast-osteoclast co-culture. (**a** and **d**) Haematoxylin and eosin overview staining showing the presence of cells throughout the construct. A dashed line shows the incision for monocyte seeding. (**b** and **e**) Von Kossa staining revealing mineralised matrix formation (in black) and mineralised SF (in brown) throughout the whole scaffold. A dashed line shows the incision for monocyte seeding. (**c** and **f**, **g**–**j**) Fluorescent composite images and individual channels showing cells expressing typical bone cell markers: osterix (osteoblast marker, red), integrin β3 (osteoclast marker, green), and sclerostin (osteocyte marker, yellow). Nuclei stained with DAPI (blue).

osteoclastic activity (Hayman, 2008; Kirstein *et al.*, 2006). TRAP samples were taken over time from the same cells, which allowed the determination of the moment of peak TRAP release. As TRAP release was elevated at day 7 in both the 2D and 3D culture, and resorption was visualised in the 2D mono-culture at day 8 after initiating the differentiation, it is reasonable to assume that osteoclasts had formed already before day 7, which would result in a projected life expectancy of 21 d. As expected, TRAP release by cells cultured on plastic decreased sharply within 3 weeks of culture. However, the TRAP release of cells cultured on a mineralised surface in 2D or on constructs in 3D continued until the end of the experiment. This suggests that the presence of a mineralised surface is sufficient to prolong the osteoclastic activity, and perhaps to extend the lifespan of osteoclasts. In 3D, in addition to the presence of a mineralised surface, other factors could have contributed to the prolonged TRAP release, such as biochemical signals released by sclerostin-expressing cells (Atkins *et al.*, 2009; Simonet *et al.*, 1997; Wijenayaka *et al.*, 2011) and osteoblasts (Matsuo and Irie, 2008). These findings are in line with the μCT data, further reinforcing the findings that resorption exceeded formation after 12 d in the osteoblast-osteoclast co-culture.

Large osteoclast-like cells (around 50 μm in diameter) were identified throughout the construct, most often in proximity to small pits. These pits are believed to be resorption pits and, although small in diameter, are within the range of sizes that others have reported in *in vitro* studies (Halai *et al.*, 2014; Kleinhans *et al.*, 2015; Varghese *et al.*, 2006). Their morphology is different from the observed resorption in the 2D culture, where resorption presented itself as classical resorption trails with a width of approximately osteoclast size (50 μm) and larger. It is likely that larger areas of resorption are present on the 3D constructs, but do not have enough distinguishing features to confirm that they are truly resorption pits or trails. Similar difficulties arise when using extracellular bone matrix of for example bovine origin (Kleinhans *et al.*, 2015). Small distinct pits can be distinguished easily, but the larger the resorbed area and the less steep the slope of the pit, the harder it is to discern on a non-flat surface whether it is an actual resorbed area or whether the feature is part of the original construct architecture, which by itself is irregularly shaped. In Fig. 3**a**, the area surrounding the small pits seems to be structurally different from the surrounding surface, with a width similar to that of the osteoclast next to it, suggesting the area surrounding the pits could be a resorption

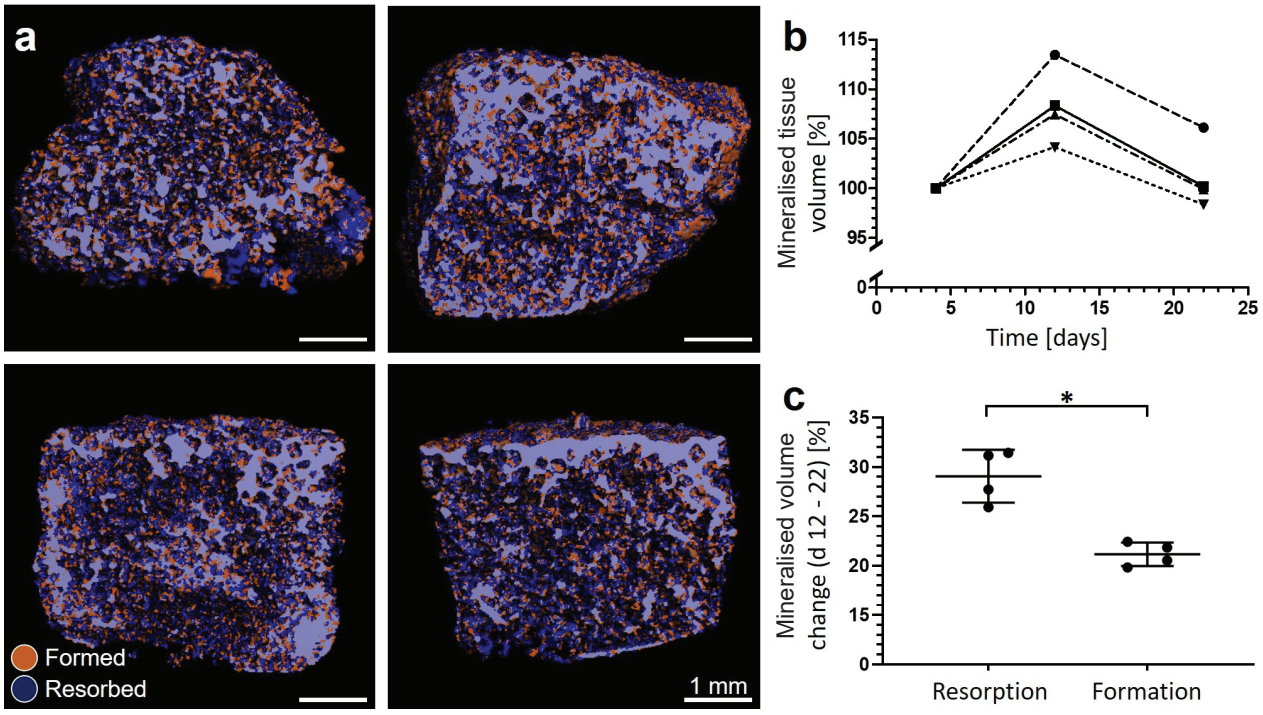

Fig. 5. Formation and resorption occurred simultaneously in the 3D osteoblast-osteoclast co-culture. (**a**) 3D μCT images of 4 constructs were registered between days 12 and 22 of co-culture, digitally cross-sectioned and color-coded to visualise the formation (orange), resorption (dark blue), and unaltered regions (grey-purple). Depth of the 3D image creates shadows that make the areas deeper inside the constructs appear darker. (**b**) The overall remodelling balance switched from mainly formation to mainly resorption after 12 d of osteoclastic differentiation. Each line represents one construct. (**c**) Both formation and resorption are present between days 12 and 22 of co-culture, as determined by the voxel count *per* colour as percentage of the total number of voxels measured at d 12. Both individual samples are plotted and their average ± SD are plotted. The difference between formation and resorption is statistically significant ($p = 0.0017$).

trail. Identification of osteoblasts on the SEM images proved difficult due to the used methodology (Shah *et al*., 2019; Wierzchos *et al*., 2008). Their presence within the constructs was confirmed by histology.

The herein presented model contains the required cells to simulate bone crosstalk but has some limitations compared to natural bone. While the original porous scaffold mimics the geometry of trabecular bone, there are many aspects that do not accurately mimic bone tissue. There is no cortical bone, bone marrow or vasculature, and there is no systemic interaction with other tissues. Cells are introduced at discrete moments, whereas in bone there can be a continuous influx of cells in response to the correct biochemical cues. In the model, osteoblasts are introduced first to deposit mineralised matrix, followed by osteoclasts to resorb the deposited matrix. As a result, the phases of the bone remodelling cycle (resorption of damaged or old bone, followed by a reversal phase and formation of new bone) are actually reversed (Delaisse, 2014). Whereas in the bone remodelling cycle osteoblasts and osteoclasts are separated by a reversal phase, the current model provides the opportunity to manipulate and study osteoblasts, osteoclasts and their interactions together within the same environment at the same time.

3D *in vitro* co-cultures are subject to certain limitations. To answer patient-specific questions using trabecular bone-like bone structures requires a large number of well characterised cells (Buenzli and Sims, 2015) preferably from a single donor or patient (Evans *et al*., 2006). While well-characterised MSCs are available because these cells can be expanded (Ferrin *et al*., 2017; Ma *et al*., 2014), the number of monocytes available from a single blood donation is limited by the donated volume and dependent on donor characteristics and state of health (Yang *et al*., 2018). Monocytes cannot naturally be expanded (Jacome-Galarza *et al*., 2013), although exposure to M-CSF (without RANKL) has been reported to allow limited expansion, accelerated differentiation and survival of monocytes (Ross, 2006; Xu and Teitelbaum, 2013; Yamada *et al*., 2005), at the risk of developing an insensitivity to RANKL (De Vries *et al*., 2015). Large between-donor variation in activity and resorption is another issue in particular in the case of monocytes (Susa *et al*., 2004) that necessitates choosing one out of several tested donors.

Future research should focus on switching from an artificial to a more physiological environment where the cells present can produce sufficient cytokines by themselves to regulate formation and resorption activity between each other to the extent that these changes are large enough to be detected using μCT, as is the case *in vivo*. This may necessitate the development of a completely functional bone remodelling unit including osteocytes, requiring additional validation of their presence and function. In future experiments, biochemical bone turnover markers such as procollagen-1 N-terminal peptide (P1NP) and C-terminal telopeptide of type I collagen (CTx) could be included to corroborate the volume-based μCT findings, and optimisation of cell seeding techniques and culture durations could reduce variation and increase throughput of the system. Further validation of the use of μCT for these experiments should be conducted, specifically regarding the effect of radiation on cell survival and activity. Certain doses of radiation can negatively affect osteoblast function (Kraehenbuehl *et al*., 2010), and may affect monocytes and osteoclasts as well (Yang *et al*., 2012). Combined with the monitoring technology, this model could provide important information on the fine balance between formation and resorption rather than just looking at the overall increase and decrease of tissue volume. The presented co-culture system is a first step towards the development of a 3D *in vitro* model that could be used for fundamental research on bone remodelling and related bone diseases. It may have clinical relevance for patient-specific disease diagnosis, therapies or drug development when used with patient-derived cells.

Conclusion

This study shows that human monocytes can differentiate into osteoclasts when co-cultured with osteoblasts differentiated from hMSCs *in vitro*. In the co-culture, both cell types are simultaneously functional, osteoblasts form and osteoclasts resorb mineralised tissue. These processes can be quantified, visualised and localised using μCT. In this way, the effect of biochemical signals, drugs and other stimuli on bone crosstalk could be studied in a 3D *in vitro* model with unprecedented similarity to human *in vivo* bone remodelling.

Acknowledgements

The authors would like to thank Sana Ansari for her assistance with confocal fluorescence microscopy. This project was supported by the European Union's Seventh Framework Programme (FP/2007-2013), Grant Agreement No. 336043 (project REMOTE).

References

Amizuka N, Takahashi N, Udagawa N, Suda T, Ozawa H (1997) An ultrastructural study of cell-cell contact between mouse spleen cells and calvaria-derived osteoblastic cells in a co-culture system for osteoclast formation. Acta Histochem Cytochem **30**: 351-362.

Atkins GJ, Welldon KJ, Halbout P, Findlay DM (2009) Strontium ranelate treatment of human primary osteoblasts promotes an osteocyte-like phenotype while eliciting an osteoprotegerin response. Osteoporos Int **20**: 653-664.

Barbeck M, Booms P, Unger R, Hoffmann V, Sader R, Kirkpatrick CJ, Ghanaati S (2017) Multinucleated giant cells in the implant bed of bone substitutes are foreign body giant cells-New insights into the material-mediated healing process. J Biomed Mater Res A **105**: 1105-1111.

Bellido T (2014) Osteocyte-driven bone remodeling. Calcif Tissue Int **94**: 25-34.

Bonito V, de Kort B, Bouten C, Smits A (2018) Cyclic strain affects macrophage cytokine secretion and ECM turnover in electrospun scaffolds. Tissue Eng Part A **25**: 1310-1325.

Buenzli PR, Sims NA (2015) Quantifying the osteocyte network in the human skeleton. Bone **75**: 144-150.

Burkhardt AM, Zlotnik A (2013) Translating translational research: mouse models of human disease. Cell Mol Immunol **10**: 373-374.

Contopoulos-Ioannidis DG, Ntzani E, Ioannidis JPA (2003) Translation of highly promising basic science research into clinical applications. Am J Med **114**: 477-484.

Delaisse J-M (2014) The reversal phase of the bone-remodeling cycle: cellular prerequisites for coupling resorption and formation. Bonekey Rep **3**: 561.

Deschaseaux F, Pontikoglou C, Sensebe L (2010) Bone regeneration: the stem/progenitor cells point of view. J Cell Mol Med **14**: 103-115.

Edmondson R, Broglie JJ, Adcock AF, Yang L (2014) Three-dimensional cell culture systems and their applications in drug discovery and cell-based biosensors. Assay Drug Dev Technol **12**: 207-218.

Ellouz R, Chapurlat R, van Rietbergen B, Christen P, Pialat J-B, Boutroy S (2014) Challenges in longitudinal measurements with HR-pQCT: Evaluation of a 3D registration method to improve bone microarchitecture and strength measurement reproducibility. Bone **63**: 147-157.

Evans CE, Mylchreest S, Andrew JG (2006) Age of donor alters the effect of cyclic hydrostatic pressure on production by human macrophages and osteoblasts of sRANKL, OPG and RANK. BMC Musculoskelet Disord **7**: 21.

Ferrin I, Beloqui I, Zabaleta L, Salcedo JM, Trigueros C, Martin AG (2017) Isolation, culture, and expansion of mesenchymal stem cells. Methods Mol Biol **1590**: 177-190.

Frost HM (1969) Tetracycline-based histological analysis of bone remodeling. Calcif Tissue Res **3**: 211-237.

Goers L, Freemont P, Polizzi KM (2014) Co-culture systems and technologies: taking synthetic biology to the next level. J R Soc Interface **11**: 20140065. doi: 10.1098/rsif.2014.0065

Hagenmüller H, Hofmann S, Kohler T, Merkle HP, Kaplan DL, Vunjak-Novakovic G, Müller R, Meinel L (2007) Non-invasive time-lapsed monitoring and quantification of engineered bone-like tissue. Ann Biomed Eng **35**: 1657-1667.

Halai M, Ker A, Meek RD, Nadeem D, Sjostrom T, Su B, McNamara LE, Dalby MJ, Young PS (2014) Scanning electron microscopical observation of an osteoblast/osteoclast co-culture on micropatterned orthopaedic ceramics. J Tissue Eng **5**: 2041731414552114. doi: 10.1177/2041731414552114. eCollection 2014

Hayden RS, Quinn KP, Alonzo CA, Georgakoudi I, Kaplan DL (2014) Quantitative characterization of mineralized silk film remodeling during long-term osteoblast-osteoclast co-culture. Biomaterials **35**: 3794-3802.

Hayman AR (2008) Tartrate-resistant acid phosphatase (TRAP) and the osteoclast/immune cell dichotomy. Autoimmunity **41**: 218-223.

Heinemann C, Heinemann S, Bernhardt A, Lode A, Worch H, Hanke T (2010) *In vitro* osteoclastogenesis on textile chitosan scaffold. Eur Cell Mater **19**: 96-106.

Hofmann S, Hagenmüller H, Koch AM, Müller R, Vunjak-Novakovic G, Kaplan DL, Merkle HP, Meinel L (2007) Control of *in vitro* tissue-engineered bone-like structures using human mesenchymal stem cells and porous silk scaffolds. Biomaterials **28**: 1152-1162.

Hofmann S, Hilbe M, Fajardo RJ, Hagenmüller H, Nuss K, Arras M, Müller R, von Rechenberg B, Kaplan DL, Merkle HP, Meinel L (2013) Remodeling of tissue-engineered bone structures *in vivo*. Eur J Pharm Biopharm **85**: 119-129.

Jacome-Galarza CE, Lee S-K, Lorenzo JA, Aguila HL (2013) Identification, characterization, and isolation of a common progenitor for osteoclasts, macrophages, and dendritic cells from murine bone marrow and periphery. J Bone Miner Res **28**: 1203-1213.

Jemnitz K, Veres Z, Monostory K, Kóbori L, Vereczkey L (2008) Interspecies differences in acetaminophen sensitivity of human, rat, and mouse primary hepatocytes. Toxicol In Vitro **22**: 961-967.

Kirstein B, Chambers TJ, Fuller K (2006) Secretion of tartrate-resistant acid phosphatase by osteoclasts correlates with resorptive behavior. J Cell Biochem **98**: 1085-1094.

Klein-Nulend J, Bacabac RG, Bakker AD (2012) Mechanical loading and how it affects bone cells: the role of the osteocyte cytoskeleton in maintaining our skeleton. Eur Cell Mater **24**: 278-291.

Klein-Nulend J, Bakker AD, Bacabac RG, Vatsa A, Weinbaum S (2013) Mechanosensation and transduction in osteocytes. Bone **54**: 182-190.

Kleinhans C, Schmid FF, Schmid F V, Kluger PJ (2015) Comparison of osteoclastogenesis and resorption activity of human osteoclasts on tissue culture polystyrene and on natural extracellular bone matrix in 2D and 3D. J Biotechnol **205**: 101-110.

Kraehenbuehl TP, Stauber M, Ehrbar M, Weber F, Hall H, Muller R (2010) Effects of μCT radiation on tissue engineered bone-like constructs. Biomed Tech (Berl) **55**: 245-250.

Kulkarni RN, Bakker AD, Everts V, Klein-Nulend J (2012) Mechanical loading prevents the stimulating effect of IL-1β on osteocyte-modulated osteoclastogenesis. Biochem Biophys Res Commun **420**: 11-16.

Li Y, Kilian KA (2015) Bridging the gap: from 2D cell culture to 3D microengineered extracellular matrices. Adv Healthc Mater **4**: 2780-2796.

Ma J, Both SK, Yang F, Cui F-Z, Pan J, Meijer GJ, Jansen JA, van den Beucken JJJP (2014) Concise review: cell-based strategies in bone tissue engineering and regenerative medicine. Stem Cells Transl Med **3**: 98-107.

Marino S, Logan JG, Mellis D, Capulli M (2014) Generation and culture of osteoclasts. Bonekey Rep **3**: 570.

Matsuo K, Irie N (2008) Osteoclast-osteoblast communication. Arch Biochem Biophys **473**: 201-209.

Meinel L, Fajardo R, Hofmann S, Langer R, Chen J, Snyder B, Vunjak-Novakovic G, Kaplan D (2005) Silk implants for the healing of critical size bone defects. Bone **37**: 688-698.

Melke J, Zhao F, van Rietbergen B, Ito K, Hofmann S (2018) Localisation of mineralised tissue in a complex spinner flask environment correlates with predicted wall shear stress level localisation. Eur Cell Mater **36**: 57-68.

Nakamura I, Duong LT, Rodan SB, Rodan GA (2007) Involvement of $\alpha v\beta 3$ integrins in osteoclast function. J Bone Miner Metab **25**: 337-344.

Nazarov R, Jin H-J, Kaplan DL (2004) Porous 3-D scaffolds from regenerated silk fibroin. Biomacromolecules **5**: 718-726.

Owen R, Reilly GC (2018) *In vitro* models of bone remodelling and associated disorders. Front Bioeng Biotechnol **6**: 134.

Pang H, Wu XH, Fu SL, Luo F, Zhang ZH, Hou TY, Li ZQ, Chang ZQ, Yu B, Xu JZ (2013) Co-culture with endothelial progenitor cells promotes survival, migration, and differentiation of osteoclast precursors. Biochem Biophys Res Commun **430**: 729-734.

Papadimitropoulos A, Scherberich A, Guven S, Theilgaard N, Crooijmans HJ, Santini F, Scheffler K, Zallone A, Martin I (2011) A 3D *in vitro* bone organ model using human progenitor cells. Eur Cell Mater **21**: 445-458.

Parfitt AM (1994) Osteonal and hemi-osteonal remodeling: The spatial and temporal framework for signal traffic in adult human bone. J Cell Biochem **55**: 273-286.

Paschos NK, Brown WE, Eswaramoorthy R, Hu JC, Athanasiou KA (2015) Advances in tissue engineering through stem cell-based co-culture. J Tissue Eng Regen Med **9**: 488-503.

Pathak JL, Bravenboer N, Luyten FP, Verschueren P, Lems WF, Klein-Nulend J, Bakker AD (2015) Mechanical loading reduces inflammation-induced human osteocyte-to-osteoclast communication. Calcif Tissue Int **97**: 169-178.

Perrotti V, Nicholls BM, Horton MA, Piattelli A (2009) Human osteoclast formation and activity on a xenogenous bone mineral. J Biomed Mater Res A **90**: 238-246.

Ross FP (2006) M-CSF, c-Fms, and signaling in osteoclasts and their precursors. Ann N Y Acad Sci **1068**: 110-116.

Samal SK, Dash M, Declercq HA, Gheysens T, Dendooven J, Voort P Van Der, Cornelissen R, Dubruel P, Kaplan DL (2014) Enzymatic mineralization of silk scaffolds. Macromol Biosci **14**: 991-1003.

Schulte FA, Lambers FM, Kuhn G, Muller R (2011a) *In vivo* micro-computed tomography allows direct three-dimensional quantification of both bone formation and bone resorption parameters using time-lapsed imaging. Bone **48**: 433-442.

Schulte FA, Lambers FM, Webster DJ, Kuhn G, Muller R (2011b) *In vivo* validation of a computational bone adaptation model using open-loop control and time-lapsed micro-computed tomography. Bone **49**: 1166-1172.

Shah FA, Ruscsák K, Palmquist A (2019) 50 years of scanning electron microscopy of bone—a comprehensive overview of the important discoveries made and insights gained into bone material properties in health, disease, and taphonomy. Bone Res **7**: 15.

Simonet WS, Lacey DL, Dunstan CR, Kelley M, Chang MS, Lüthy R, Nguyen HQ, Wooden S, Bennett L, Boone T, Shimamoto G, DeRose M, Elliott R, Colombero A, Tan HL, Trall G, Sullivan J, Davy E, Bucay N, Renshaw-Gegg L, Hughes TM, Hill D, Pattison W, Campbell P, Sander S, Van G, Tarpley J, Derby P, Lee R, Boyle WJ (1997) Osteoprotegerin: A novel secreted protein involved in the regulation of bone density. Cell **89**: 309-319.

Sims NA, Gooi JH (2008) Bone remodeling: Multiple cellular interactions required for coupling of bone formation and resorption. Semin Cell Dev Biol **19**: 444-451.

Susa M, Luong-Nguyen N-H, Cappellen D, Zamurovic N, Gamse R (2004) Human primary osteoclasts: *in vitro* generation and applications as pharmacological and clinical assay. J Transl Med **2**: 6.

Tang Y, Wu X, Lei W, Pang L, Wan C, Shi Z, Zhao L, Nagy TR, Peng X, Hu J, Feng X, Van Hul W, Wan M, Cao X (2009) TGF-β1–induced migration of bone mesenchymal stem cells couples bone resorption with formation. Nat Med **15**: 757-765.

Tsukada M, Gotoh Y, Nagura M, Minoura N, Kasai N, Freddi G (1994) Structural changes of silk fibroin membranes induced by immersion in methanol aqueous solutions. J Polym Sci [B] **32**: 961-968.

Varghese BJ, Aoki K, Shimokawa H, Ohya K, Takagi Y (2006) Bovine deciduous dentine is more susceptible to osteoclastic resorption than permanent dentine: results of quantitative analyses. J Bone Miner Metab **24**: 248-254.

De Vries TJ, Schoenmaker T, Aerts D, Grevers LC, Souza PPC, Nazmi K, van de Wiel M, Ylstra B, Lent PL Van, Leenen PJM, Everts V (2015) M-CSF priming of osteoclast precursors can cause osteoclastogenesis-

insensitivity, which can be prevented and overcome on bone. J Cell Physiol **230**: 210-225.

Wierzchos J, Falcioni T, Kiciak A, Woliński J, Koczorowski R, Chomicki P, Porembska M, Ascaso C (2008) Advances in the ultrastructural study of the implant–bone interface by backscattered electron imaging. Micron **39**: 1363-1370.

Wijenayaka AR, Kogawa M, Lim HP, Bonewald LF, Findlay DM, Atkins GJ (2011) Sclerostin stimulates osteocyte support of osteoclast activity by a RANKL-dependent pathway.. PLoS One **6**: e25900. doi: 10.1371/journal.pone.0025900

Xian L, Wu X, Pang L, Lou M, Rosen CJ, Qiu T, Crane J, Frassica F, Zhang L, Rodriguez JP, Jia X, Yakar S, Xuan S, Efstratiadis A, Wan M, Cao X (2012) Matrix IGF-1 maintains bone mass by activation of mTOR in mesenchymal stem cells. Nat Med **18**: 1095-1101.

Xu F, Teitelbaum SL (2013) Osteoclasts: new insights. Bone Res **1**: 11-26.

Yamada N, Tsujimura T, Ueda H, Hayashi S-I, Ohyama H, Okamura H, Terada N (2005) Down-regulation of osteoprotegerin production in bone marrow macrophages by macrophage colony-stimulating factor. Cytokine **31**: 288-297.

Yang B, Zhou H, Zhang X-D, Liu Z, Fan F-Y, Sun Y-M (2012) Effect of radiation on the expression of osteoclast marker genes in RAW264.7 cells. Mol Med Rep **5**: 955-958.

Yang J, Qiao M, Li Y, Hu G, Song C, Xue L, Bai H, Yang J, Yang X (2018) Expansion of a population of large monocytes (atypical monocytes) in peripheral blood of patients with acute exacerbations of chronic obstructive pulmonary diseases. Mediators Inflamm **2018**: 1-13.

Zhu S, Ehnert S, Rouß M, Häussling V, Aspera-Werz RH, Chen T, Nussler AK (2018) From the clinical problem to the basic research—co-culture models of osteoblasts and osteoclasts. Int J Mol Sci **19**: 2284.

Discussion with Reviewers

Katharina Jähn: Some biomaterials, particularly when cultured for long periods, present difficulties in the subsequent extraction of good quality RNA. Do the authors know if their mineralised silk-fibroin scaffold is amenable to RNA extraction following long culture periods (*e.g.* > 4 weeks)?
Authors: Earlier (unpublished) experiments in our lab have shown the same difficulties in extracting good quality RNA from highly mineralised silk fibroin scaffolds. It is for that reason that alternative methods of quantification are of such importance.

Katharina Jähn: Regarding refinement of the model system, how do the authors anticipate resolving the issue of reliable monocyte seeding without the need to cut the scaffold?
Authors: The main challenge in seeding monocytes lies in the time they need to attach to a surface. The optimal duration for these cells to attach has not been accurately determined in the literature and may show between-donor variation. Our experiment approached this challenge in the 'safest' way possible; by putting the monocytes where they are wanted and by keeping them there long enough to attach before adding additional culture medium. The authors agree that more refined and reproducible methods would be preferable.

Alternative methods are currently under investigation. One such method is orbital seeding, which has been studied in our lab for seeding MSCs recently (Additional reference: Melke *et al*., 2020). Another method under investigation is to use flow-perfusion bioreactors for seeding the monocytes. While more refined than the current method, both proposed methods result in a considerable loss of cells of an already limited number of cells available *per* blood donation. Once an optimal seeding density has been determined using the current method and the between-donor variation can be accounted for, our aim is to continue with one of the two suggested seeding methods.

Keith Thompson: Can the authors comment on the potential to incorporate osteocytes / or generate osteocytes by means of osteoblast-to-osteocyte differentiation in their 3D co-culture?
Authors: We agree with the reviewer that this system is far from showing all functionalities of the bone remodelling process, and in particular the presence of osteocytes. To provide this, the aim should be to include osteocytes as orchestrators of bone remodelling into this system. Achieving this will also add another layer of complexity to the system. The most straight-forward way to integrate osteocytes would be to start with MSC differentiation into osteoblasts followed by differentiating most of them further into osteocytes while keeping osteoblasts/lining cells on the surface. It is particularly challenging to define from which time points cells have reached the mature osteocyte differentiation stage and even more so, whether they are functional. Are they embedded in the lacuna-canalicular system? Do they exhibit the typical morphology and connect with each other and the bone surface? Will they produce/express the correct signals in response to mechanical loads? When is the ideal timing to (re) introduce osteoclasts (or their progenitors) and should they be introduced in sequence or in parallel?

Additional Reference

Melke J, Zhao F, Ito K, Hofmann S (2020) Orbital seeding of mesenchymal stromal cells increases osteogenic differentiation and bone-like tissue formation. J Orthop Res **38**: 1228-1237

Editor's note: The Scientific Editor responsible for this paper was Martin Stoddart.